SANDIA REPORT

SAND2012-8468
Unlimited Release
Printed October 2012

Equation of state of CO_2: experiments on Z, density functional theory (DFT) simulations, and tabular models

Seth Root, John H. Carpenter, Kyle R. Cochrane, Thomas R. Mattsson

Prepared by
Sandia National Laboratories
Albuquerque, New Mexico 87185 and Livermore, California 94550

Sandia National Laboratories is a multi-program laboratory managed and operated by Sandia Corporation, a wholly owned subsidiary of Lockheed Martin Corporation, for the U.S. Department of Energy's National Nuclear Security Administration under contract DE-AC04-94AL85000.

Approved for public release; further dissemination unlimited.

Sandia National Laboratories

Issued by Sandia National Laboratories, operated for the United States Department of Energy by Sandia Corporation.

NOTICE: This report was prepared as an account of work sponsored by an agency of the United States Government. Neither the United States Government, nor any agency thereof, nor any of their employees, nor any of their contractors, subcontractors, or their employees, make any warranty, express or implied, or assume any legal liability or responsibility for the accuracy, completeness, or usefulness of any information, apparatus, product, or process disclosed, or represent that its use would not infringe privately owned rights. Reference herein to any specific commercial product, process, or service by trade name, trademark, manufacturer, or otherwise, does not necessarily constitute or imply its endorsement, recommendation, or favoring by the United States Government, any agency thereof, or any of their contractors or subcontractors. The views and opinions expressed herein do not necessarily state or reflect those of the United States Government, any agency thereof, or any of their contractors.

Printed in the United States of America. This report has been reproduced directly from the best available copy.

Available to DOE and DOE contractors from
U.S. Department of Energy
Office of Scientific and Technical Information
P.O. Box 62
Oak Ridge, TN 37831

Telephone: (865) 576-8401
Facsimile: (865) 576-5728
E-Mail: reports@adonis.osti.gov
Online ordering: http://www.osti.gov/bridge

Available to the public from
U.S. Department of Commerce
National Technical Information Service
5285 Port Royal Rd
Springfield, VA 22161

Telephone: (800) 553-6847
Facsimile: (703) 605-6900
E-Mail: orders@ntis.fedworld.gov
Online ordering: http://www.ntis.gov/help/ordermethods.asp?loc=7-4-0#online

SAND2012-8468
Unlimited Release
Printed October 2012

Equation of state of CO_2: experiments on Z, density functional theory (DFT) simulations, and tabular models

Seth Root[1], John H. Carpenter[2], Kyle R. Cochrane[3], and Thomas R. Mattsson[3]
[1]Dynamic Material Properties, [2]Computational Shock and Multiphysics,
and [3]HEDP Theory
Sandia National Laboratories
P.O. Box 5800
Albuquerque, NM 87185-1189

Abstract

Over the last few years, first-principles simulations in combination with increasingly accurate shock experiments at multi-Mbar pressure have yielded important insights into how matter behaves under shock loading. Carbon dioxide (CO_2) is particularly interesting to study as a model molecular system for planetary science. Under high pressure - high temperature CO_2 dissociates and eventually begins ionizing. The dissociation pathway and the equation of state at extreme conditions is poorly understood. Cryogenic CO_2 is optically transparent while shocked CO_2 is metallic, displaying a reflective shock front, thus allowing for shock velocity measurement to very high precision. In this report, we present experimental results for shock compression of liquid cryogenic CO_2 to several Mbar using magnetically accelerated flyers on the Z machine, first-principles simulations based on Density Functional Theory including examining the CO_2 dissociation pathway, and an analysis of tabular equations of state (EOS) for CO_2.

Acknowledgment

We sincerely thank the many devoted specialists with Z-Operations who are involved in planning and executing experiments on the Z-machine. We thank the cryogenic team: Andrew Lopez, Keegan Shelton, and Jose Villalva for installing and running the cryostat. We thank Aaron Bowers, Nicole Cofer, and Jesse Lynch for assembling the cryo-targets. We thank Charlie Meyers for running the VISAR diagnostics and Devon Dalton for handling target design.

Contents

Nomenclature **8**

1 Introduction **9**

2 DFT Simulations of Shock Compressed CO_2 **13**

3 Multi-Mbar shock experiments on Z **21**

4 Analysis of CO_2 tabular EOS models **29**

4.1 Shock Compression 29

4.2 Fluid Isobars 31

4.3 Phase boundaries 32

4.4 Recommendations 32

5 Summary **35**

References **36**

List of Figures

1.1 Xenon as an example of significant differences between EOS models. 10

1.2 The previous Hugoniot data and tabular EOS models for liquid carbon dioxide. . . . 11

1.3 The Z machine at Sandia National Laboratories. 11

2.1 Typical simulation 14

2.2 Time dependent pressure averaging 15

2.3 Measure of the Rankine-Hugoniot relation 16

2.4 Inflection along the Hugoniot in ρ-T space 17

2.5 CO_2 dissociation along the Hugoniot 20

3.1 Experimental setup 22

3.2 Phase diagram of CO_2 23

3.3 Schematic view of the flyer-plate impact experiment 24

3.4 Comparison of reflected Hugoniot and DFT calculated quartz release paths 26

3.5 $U_S - U_P$ Hugoniot data 27

3.6 $\rho - P$ Hugoniot data 28

4.1 Shock compression results 30

4.2 Shock temperature results 30

4.3 Isobaric expansion of fluid 31

4.4 Vaporization results 33

List of Tables

2.1 Hugoniot from VASP simulations using the AM05 potential. 18

3.1 Cubic fit parameters for the Z-quartz Hugoniot 25

3.2 Linear fit parameters to the C-cut sapphire Hugoniot 25

3.3 Experimental data of the principal Hugoniot for shock compressed liquid CO_2 26

4.1 Critical points 32

Nomenclature

DFT Density Functional Theory

EOS Equation of State

VISAR Velocity Interferometer System for Any Reflector

Chapter 1

Introduction

Precise knowledge of the behavior of elements, compounds, and materials under shock compression was for decades limited to the pressures that could be achieved using guns and high explosives. On the theoretical side, electronic structure methods based on quantum mechanics were applied to calculate energy and pressure as a function of compression for perfect lattices (the so called cold curve) but dynamic simulations at temperature were limited to basic model systems like hard/soft spheres or discrete systems (ising models) etc. It was therefore, for a long time, exceedingly challenging to predict the behavior of materials much above 1 Mbar. The difficulty in extrapolating equation of state (EOS) models beyond pressures where experimental data, or high-fidelity simulations, is available is illustrated in Fig. 1.1 taken from Reference [1]. For xenon, EOS models predating our work begin to differ notably above 100 GPa and this behavior is by no means limited to xenon. On the contrary, EOS tables of many other elements and compounds exhibit similar discrepancies when different EOS models are extrapolated beyond the range in density and pressure where data is available.

In dramatic contrast to earlier capabilities, over the last few years, increasingly accurate shock experiments at multi-Mbar pressure together with first-principles simulations have resulted in greatly improved knowledge of how matter behaves under extreme conditions. For light elements like hydrogen/deuterium [2, 3] and carbon[4] the agreement between simulations and experiments is remarkable, prompting an interest in investigating also elements beyond the second row in the period table with similar high-fidelity methods.

In earlier work on xenon, we performed density functional theory (DFT) based quantum molecular dynamics (QMD) simulations, high-precision shock experiments, and developed a new tabular equation of state [1]. In this report, we expand our examination of cryogenically cooled gases and present the results for liquid CO_2. CO_2 is of interest because it is a simple molecule with different atomic constituents. The behavior of CO_2 is not known experimentally beyond approximately 100 GPa under shock conditions and existing equation of state models differ significantly above pressures near 50 GPa. Figure 1.2 shows the experimental data and tabular EOS models known prior to completing this work demonstrating the issues with the current tabular EOS models. Also observed in the experimental data is a bend in the Hugoniot starting at approximately 50 GPa, which has been attributed to dissociation. We will briefly describe very recent experiments and first-principles simulations aimed at increasing the understanding of CO_2 under high pressure, including the dissociation pathway. We will also analyze the accuracy of four available EOS tables for CO_2.

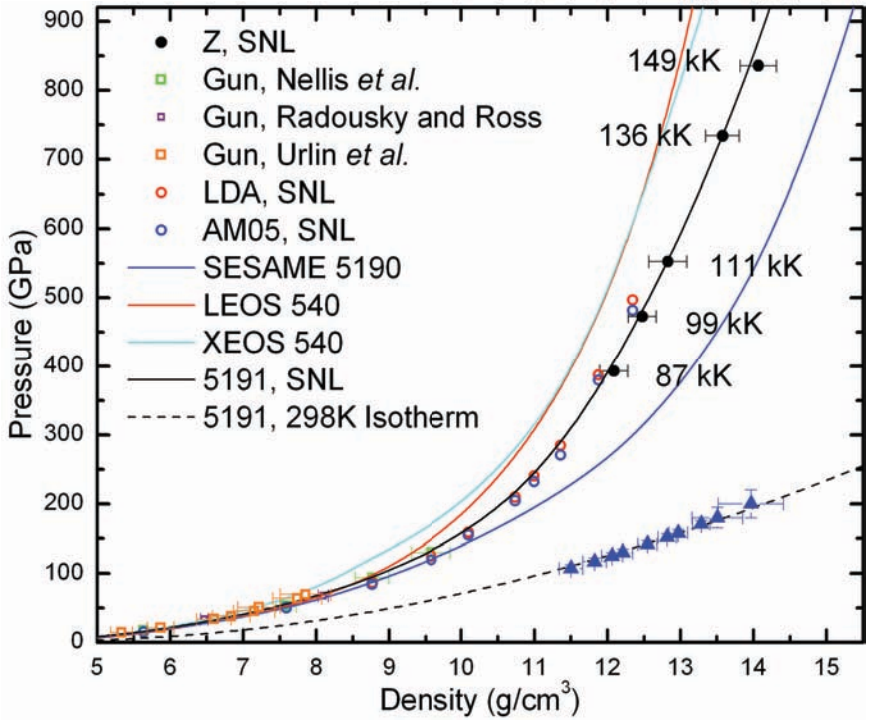

Figure 1.1. Principal Hugoniot for xenon: different tabular EOS models differ significantly above 100 GPa. Our previous work [1] resulted in a new tabular EOS (5191) based on thermodynamic data, DFT/QMD simulations, and multi-Mbar experimental data from Z. The blue triangles are isothermal compression data on solid xenon

In the first chapter, we present the computational approach for obtaining thermodynamic data from first-principles using DFT. Results from DFT simulations of carbon dioxide under high-pressures and high temperatures, completes the chapter. In chapter two, we describe multi-Mbar shock experiments performed on Sandia's Z machine, including the experimental results for CO_2 and compare the results to the prior tabular EOS models and the available DFT simulation results. The experimental discussion is followed by a chapter analyzing the accuracy of four available EOS tables for CO_2. The last section has concluding remarks.

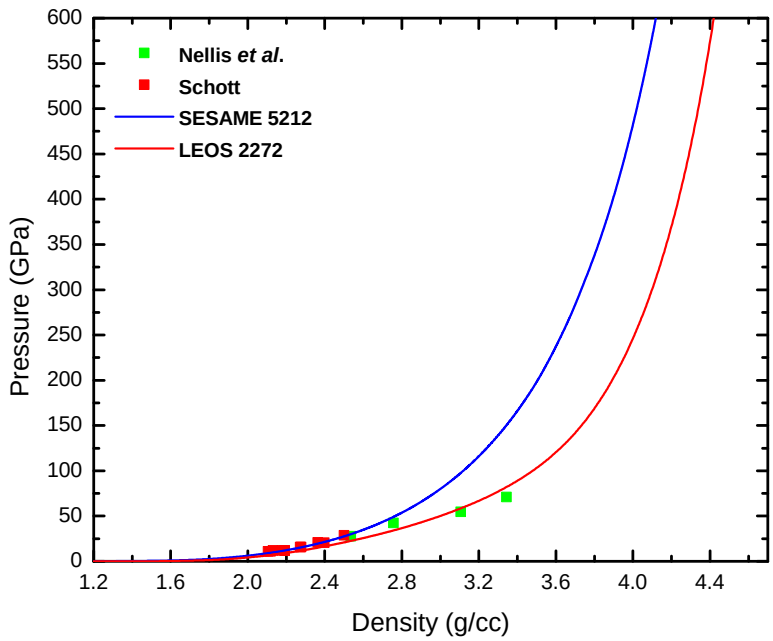

Figure 1.2. The previous Hugoniot data and tabular EOS models for liquid carbon dioxide.

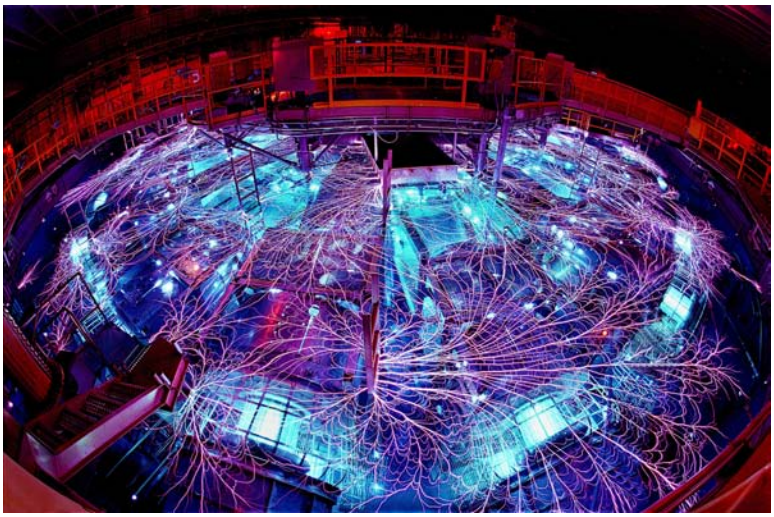

Figure 1.3. The Z machine at Sandia National Laboratories is a unique facility among the DOE complex that is utilized to produce high accuracy measurements of properties of matter under extreme conditions.

Chapter 2

DFT Simulations of Shock Compressed CO_2

Density Functional Theory (DFT) [5, 6] is based on quantum mechanics and is a widely used method to calculate the electronic structure of atoms, molecules, and solids. In DFT, the fundamental property is the density of electrons in three-dimensional real space, $\rho(x,y,z)$, regardless of how many electrons are in the system. This reformulation of the Schrődinger equation from many-body wave-functions to density makes DFT calculations very fast/efficient and it is possible to calculate properties of several hundred atoms.

DFT was for a long time employed in solid-state physics and surface science but its usefulness has with time extended into many other fields of physics. In high-energy density physics (HEDP), the breakthrough came when it was possible to perform high-precision calculations of thermodynamic quantities like internal energy and pressure [3]. Today, DFT is extensively used in HEDP and shock-physics.

The DFT-MD simulations were made with VASP 5.1.40 using projector augmented wave (PAW) core potentials and stringent convergence settings. We employed the standard potentials (PAW C8Apr2002 and PAW O8Apr2002) at a plane wave cutoff of 900 eV and complex k-point sampling with the mean-value point $(\frac{1}{4},\frac{1}{4},\frac{1}{4})$. Electronic states were occupied according to Mermin's finite-temperature formulation of DFT [7]. We have used two complementary exchange-correlation functionals: the local density approximation (LDA) and the Armiento-Mattsson (AM05) functional. AM05 includes the generalized gradient in addition to the density and is designed to capture the effects of inhomogeneity by matching results for an Airy gas. AM05 has demonstrated high fidelity for wide classes of solids under normal conditions and was recently successfully applied to study quartz to 1.7 TPa under shock compression. The principal Hugoniot is calculated with respect to a given reference state, a density of 1.173 $\frac{g}{cm^3}$ at 216 Kelvin for liquid CO_2; similar to the experimental initial conditions. The hydrostatic Hugoniot condition is expressed a 2(E-Eref) = (P+Pref) (Vref-V) with E the internal energy per atom, P the system pressure, V the volume per atom. Eref and Pref are the energy and pressure of the reference state.

The reference simulation used 64 molecues (Fig. 2.1) and was run for 4 picoseconds(ps) to ensure the mean reference pressure and energy were equilibrated to less than $\frac{1}{2}$% standard deviation. The average pressure and energy were found using block averaging [8] to reduce correlation as shown in Fig. 2.2. At low densities and temperatures, the simulations were run for multiple picoseconds at a 0.5 fs time step. At higher densities and temperatures, this time step was reduced to keep the number of electronic iterations per time step between 4 and 6. We found that if the elec-

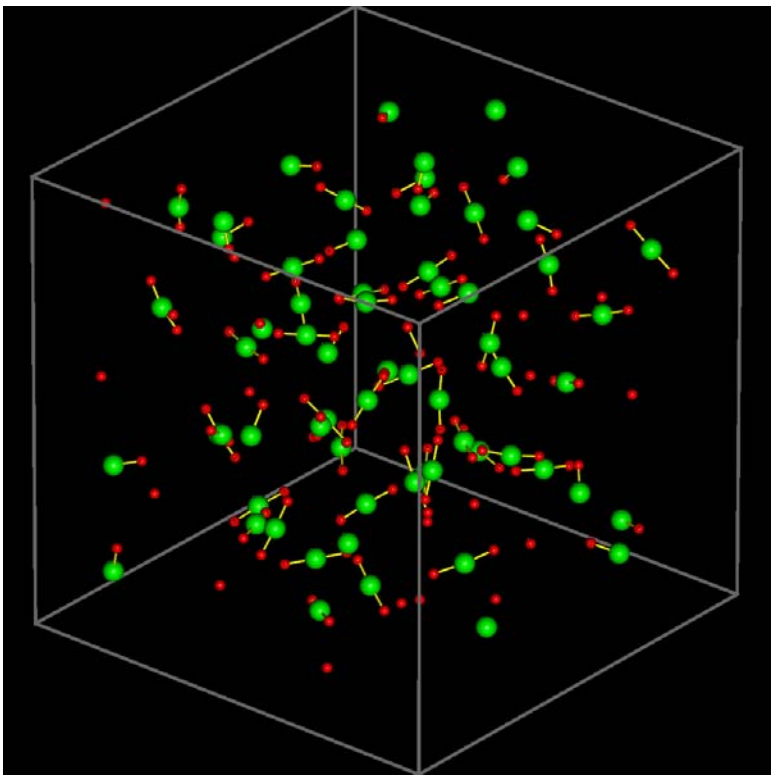

Figure 2.1. Typical 64 molecule simulation in a periodic rectilinear box. Green is carbon and red is hydrogen. The free floating atoms are across a periodic boundary, so the bonds are not drawn in those cases.

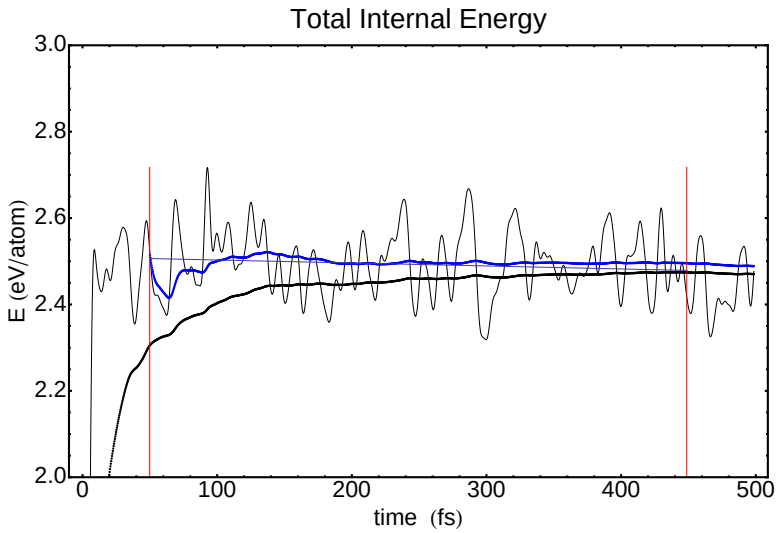

Figure 2.2. The black, highly oscillatory line, is the electronic pressure calculated by VASP. The smoother black line is a running average of the pressure. The blue line is a cumulative average and the red lines are where the block averaging begins and ends. The cumulative and block averaging start later in time because VASP simulations that are not started with a complete restart (same WAVECAR as well as CONTCAR) have an initial ring and takes some time to begin reaching equilibrium.

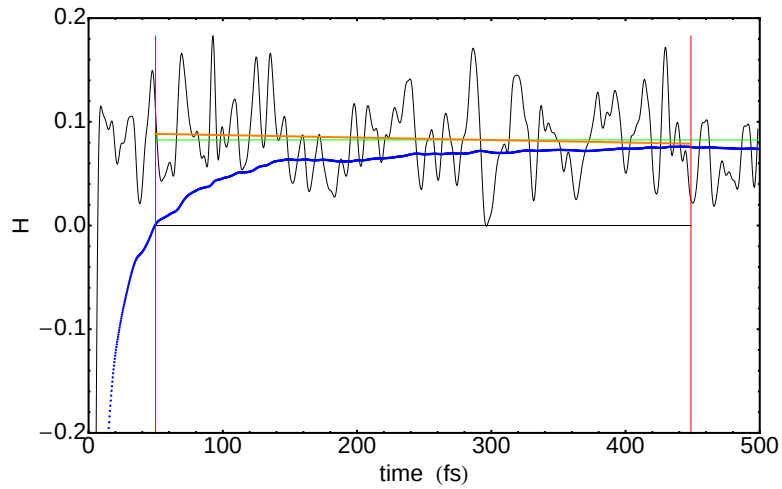

Figure 2.3. Sample of the Hugoniot relation. This figure shows the time dependent solving of the Rankine-Hugoniot relation as the simulation approaches a steady-state solution. The highly oscillatory black line is $H = 2(E - Eref) - (P + Pref)(Vref - V)$ as a function of time. The blue line is the running average of H. The red lines are the boundaries of the block averaging where the actual mean and block averaging values of H are taken. The green line is mean H. The orange line is the fit to the time dependent H. This is useful if we are ramping the temperature to more quickly find where H=0 is true and also helps determine if we have reached a steady solution based on the magnitude of the slope. The thin black line at 0 is simply to help show if the solution above or below so we know how to adjust the temperature.

tronic iteration count got above 8, the simulation would often crash many hundreds of ionic steps later because the ions were allowed to move too far in a single time step and eventually took the simulation to an ill-posed super-cell (a symptom of this is widely oscillating number of electronic iterations).

At each point along the Hugoniot, we would run at least two simulations. The simulations' temperatures were set such that the Hugoniot relation would have one point above and one point below where the Hugoniot relation was true as shown in Fig. 2.3. The actual Hugoniot point would then be interpolated between them. We bracketed the Hugoniot point because extrapolation does not work well especially around phase transitions (melt) as the pressure and energies around are often non-linear. Also, if the temperatures are too far from the Hugoniot point, then the interpolated value can be farther from the actual value than expected. The size of this window is material and Hugoniot location dependent but for most materials, ± 0.1 appears to be maximum. For example, the $1.9\frac{g}{cm^3}$ 630 Kelvin Hugoniot point was interpolated from a 600 Kelvin and 700 Kelvin simulation. The $3.8\frac{g}{cm^3}$ simulations were at 35,000 Kelvin and 36,000 Kelvin. And while this bracket is a bit larger than normal, the simulations showed we were in a gas regime such that it was adequate, primarily because we also ran 34,500 Kelvin and found a 1% difference in the

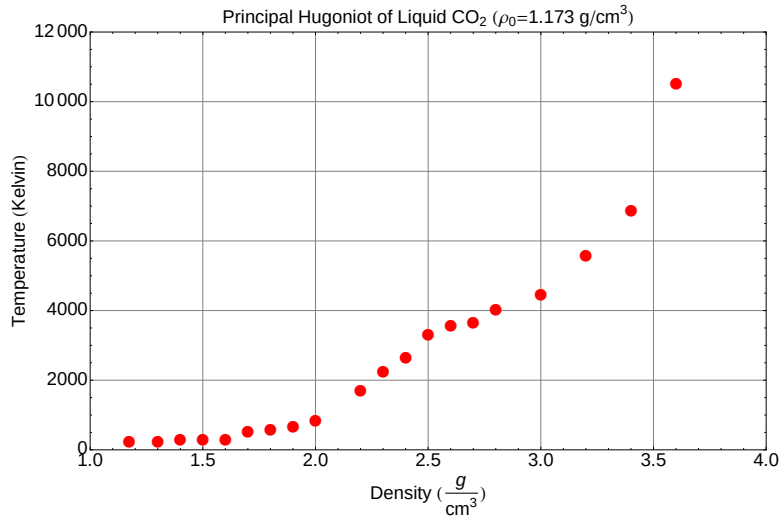

Figure 2.4. This figure shows the Hugoniot in density-temperature space. An inflection can be seen for densities between 2.5 and 3.0 $\frac{g}{cm^3}$. The inflection is associated with molecular dissociation.

interpolated Hugoniot pressure. When looking for dissociation of polymers, we usually tighten those tolerances to ± 0.01 or less if possible. At high compression, when the Hugoniot is almost independent of density, we vary the density at a fixed temperature and interpolate in density. In the high density cases, we used $0.1\frac{g}{cm^3}$ initially, but converge to a $0.05\frac{g}{cm^3}$ bracket once we have a good approximation for where the Hugoniot is.

Because the number of bands goes up with temperature thereby increasing the simulation solve time, keeping 64 molecules in the simulation for a clearly gas/liquid regime appeared to be excessive. We reduced the number of molecules to 32 and checked the pressure and energy values of the simulation. After three times compressed, we found very little difference between the larger and smaller simulations and so did much of the higher density Hugoniot with 32 molecules. We spot checked occasionally to ensure that simulations with smaller numbers of atoms still matched those with 64.

Because we set the temperature, our simulations are referred to as NVT (fixed number of atoms, volume, and prescribed temperature). One of the other methods available in VASP is NVE (fixed number of atoms, volume, and prescribed energy), but is not used in this case. As such, we can report the temperature used as part of the Hugoniot even though the temperature is not used in the Rankine-Hugoniot relation. These results are listed in Table 2.1.

Figure 2.4 shows the Hugoniot in temperature as a function of density. The inflection point between 2.5 $\frac{g}{cm^3}$ and 3.0 $\frac{g}{cm^3}$ is from molecular dissociation. Tracking bonds in a simulation is a three step process. First we determine bond lengths, then we determine bond times. Finally we

Table 2.1. Hugoniot from VASP simulations using the AM05 potential.

Density	Pressure	Energy	Temperature
kg/m^3	kBar	eV/atom	Kelvin
1.173	4.36154	-7.30764	218
1.3	8.47	-7.2995	223
1.4	10.3	-7.2922	280
1.5	15.4	-7.2797	265
1.6	19.8	-7.2659	270
1.7	33.6	-7.2314	508
1.8	40.2	-7.2071	562
1.9	51.9	-7.1682	636
2.0	72.3	-7.15130	815
2.2	153	-6.70232	1670
2.3	186	-6.65415	2232
2.4	233	-6.52059	2612
2.5	285	-6.31289	3301
2.6	314	-6.17437	3535
2.7	351	-6.04739	3642
2.8	383	-5.85049	4019
3.0	439	-5.55944	4443
3.2	560	-4.99021	5559
3.4	703	-4.30590	6848
3.6	1127	-2.80282	10502
3.8	2655	4.60769	35089
4.0	4883	15.07915	63342

identify and track the bonded atoms. The number of possible species pair combinations is

$$possible\ binary\ species\ combinations = \frac{(S+1)S}{2} \tag{2.1}$$

where S is the number of species. For this paper, we assumed this was also the number of possible bond lengths allowed. The simulations were run for picoseconds such that the atoms would have time to diffuse away from their neighbors if they were not bonded. An atom pair is considered bonded if they remain within the prescribed distance for longer than the prescribed time. Using the first minimum from the pair correlation functions of the reference simulation, 1.35 Å was used for C-O bond length. 1.60 Å for C-C and 1.6 Å for O-O were chosen from a different simulations. These bond lengths may not be the same as published results because we are using a code which takes a finite step, moving ions classically, and the extra distance takes into account atomic vibrations, allowing the atoms to move farther than the average bond length while still being ”bonded”. In the O-O case, normal bond length is 1.21 Å but we found that on our time

scales and at these temperatures, it was not relevant.

Once bond lengths are determined, the approach to tracking bonds is straight forward. First, we calculate the distance from each atom to every other atom setting up an NxN matrix in which N is the number of atoms in the simulation. Next, we compare distances between atoms to their respective bond length cutoffs. If the distance between atoms is less than the prescribed bond length, then the tally for that atom-atom combination is incremented, otherwise the tally is set to zero and must start incrementing anew. Once the tally reaches a user defined value, in our case 90 fs divided by the time step, the atoms are considered bonded. Bonds can be broken and reformed multiple times during a simulation.

Next, assuming we have some atoms that are bonded, we apply a recursive relation, following all atoms that are bonded to the initial atom and all atoms bonded to those atoms, etc. The recursive function calls end when no other bonded pairs can be traced back to the initial atom. We then examine our second atom. For clarity, the algorithm described above and shown below is not optimized.

```
void frog(vector<int> &mol, boost::multi_array<int,2> &bond, unsigned int j)
{
  bond[j][j] = -1;
  for(unsigned int k=0; k<bond.shape()[1]; k++) {
    if(bond[j][k] == 1 && bond[k][k] != -1) {
      mol.push_back(k);
      bond[j][k] = -1;
      bond[k][j] = -1;
      frog(mol,bond,k);
    }
  }
return;
}

for(j=0; j<n_atoms; j++){
    mol.clear();
    if(mbond[j][j] > -1) {
      mol.push_back(j);
      frog(mol,mbond,j);
      mol = unique(sort(mol));
      ...
```

For ease of coding and reading code, we set up a second matrix, $bond[N][N]$, such that if the bond exists for the required time or longer, then $bond[j][k] = 1$ (bonded) else $bond[j][k] = 0$ (not bonded). If an atom has already been accounted for by the bond tracking algorithm, then $bond[j][k] = bond[k][j] = -1$ and $bond[j][j] = -1$.

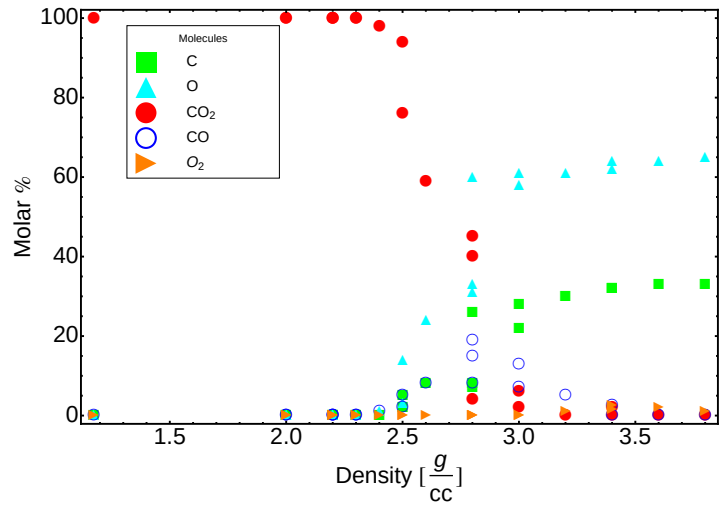

Figure 2.5. This is the dissociation of CO_2 as a function of density along the Hugoniot. The red is the molar fraction of CO_2 and is shown to be 100% at lower densities and temperature. At about 2.4 or 2.5 $\frac{g}{cm^3}$, the molecules start to dissociate and other species begin to emerge. There is a small but measurable amount of O_2 and a transient amount of CO, but by 3.5 $\frac{g}{cm^3}$, the simulation has become purely carbon and oxygen. Because we ran several temperatures at the same density in order to bracket the Hugoniot, there are several densities shown in this figure with multiple molar fractions. These are the different simulations at their different temperatures.

After the tracking phase at a given time step, we have an array listing the bonded atoms. The next step is to map each uniquely described element to its actual species. This is straight forward with strings. To simplify the process further, we used single letter descriptions such as species 1 = A and species 2 = B. This string of letters can be sorted, counted, combined ("A2B6"), and stored as an item in another array of strings (molecule). In a hydrocarbon system, the A2B6 corresponds to ethane and this mapping is done later.

In stable systems, almost any required bond time chosen will return the same answer, but in metastable simulations, the atoms can be bonded for some amount of time, move, and then rebond either to the same atoms or different ones. Therefore, as time required for the bonds to be counted goes to infinity, the reported molecules will often be just the base elements. As such, once the CO_2 starts to break up, we look for inflections or plateaus in the amounts of various marker species such as C, C_2, C_3, and O_2 in several of the transition simulations. We sampled bond times from 80 fs to 140 fs and found a slight inflection between 80 fs and 100 fs in C-O. As such, we assumed a bond time for all simulations of between 80 and 100 fs. The results are shown in Figure 2.5 where the CO_2 starts breaking down between 2.4 and 2.5 $\frac{g}{cm^3}$, and is mostly dissociated around 3.0 $\frac{g}{cm^3}$ which is in agreement with the inflection we saw in the density-temperature plot of the Hugoniot.

Chapter 3

Multi-Mbar shock experiments on Z

The Z-accelerator at Sandia [9] has been used to study properties of shocked materials for over a decade and the approach has been successively refined. Current pulses of up to 26 MA are carefully tailored to produce shock-less acceleration of flyer plates to very high impact velocities. Figure 3.1 shows the experimental setup in the Z machine center-section. The target load consists of an asymmetric coaxial load with a 9 mm X 2 mm cathode stalk. The panels have two cryo-targets (a re-established capability for Z) and the asymmetric cathode-anode (AK) gap (1 mm and 1.4 mm) provides two Hugoniot state measurements in one experiment. The cryo-targets are insulated from the load panels using nylon spacers and the targets are held in place using a nylon press piece. All targets utilized 6061-T6 aluminum flyer plates diamond machined to 1 mm in thickness.

Experimentally CO_2 provides some technical challenges not faced in previous cryogenic work such as xenon and krypton [1, 10]. With the noble gases, cooling the sample targets to temperature was all that was needed. In the case of CO_2 creating an initial liquid state requires higher pressure in addition to cooling as seen in the phase diagram shown in Figure 3.2. The need for higher pressure required modification to the target cells that were used in previous experiments on cryogenically cooled noble gases. The modified CO_2 target is viewed schematically in Fig. 3.3. To handle the high pressures, the front drive plate was made of sapphire instead of quartz. In most cases, the front drive plate was a two-piece top-hat consisting of a c-cut sapphire window to hold the pressure and a smaller z-cut alpha quartz window between the sapphire and the liquid CO_2. The rear top-hat was similarly constructed of a sapphire window to hold pressure and a smaller quartz window to interface with the sample. The thickness of sapphire windows used are capable of handling pressures in excess of 150 PSI. The use of quartz provided an accurate method for determining the Hugoniot state and the reshock state (not discussed here) in the CO_2. All window pieces were supplied by Argus International. The space between the top-hats was filled with high purity CO_2 gas (Matheson Trigas Research Purity $> 99.999\%$) to a pressure of 8.97 bar (130 PSI).

The mini-cryostat design [11] was used cool to a dual cell configuration target (see Fig 3.1) The cryostat utilized a 6061-T6 aluminum cold finger. The targets were connected to the cryostat through two copper flex links and a 14 inch long and 0.5 inch diameter copper cold rod. The cold rod was shielded using a copper tube wrapped with copper liquid nitrogen lines. The target cells were filled to 130 PSI initial (approximately 9 bar) and cooled to 220 K with liquid nitrogen. The initial liquid density of CO_2 was 1.167 g/cm^3 determined from the pressure - temperature data in Reference 12. The index of refraction is 1.272 determined from an extrapolation of the data in Reference 13. The window surfaces in contact with the liquid CO_2 were coated with an

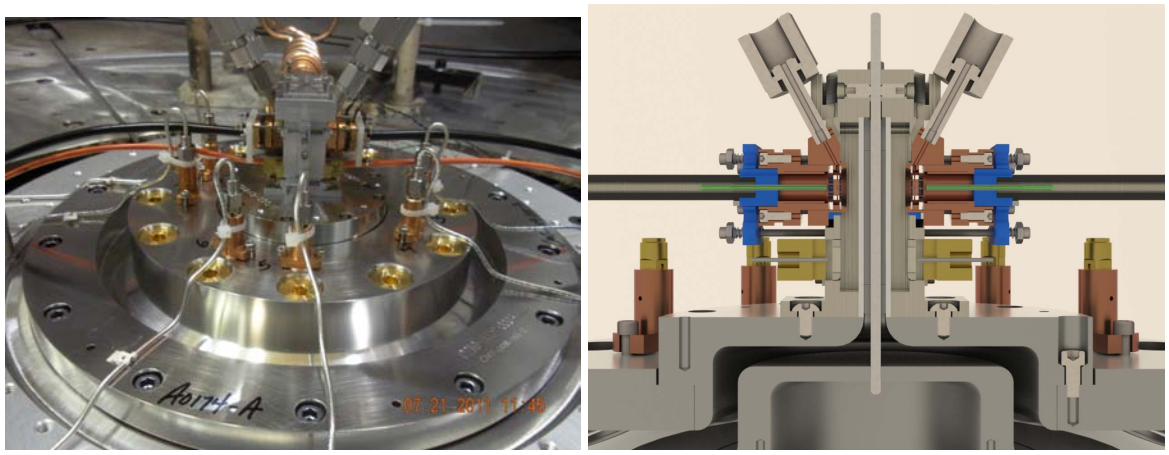

Figure 3.1. Left: An image of the experimental setup at Z. Gas lines and the cold rod from the cryostat are visible in the image. Right: A cross-sectional view of the target assembly showing the dual target assembly

anti-reflection layer to match refractive indices boundaries.

The primary diagnostic for the experiments was velocity interferometry (VISAR) [14]. The target is shown schematically on the left in Fig. 3.3. With all transparent windows, the 532nm laser for the VISAR passed through the target cell and reflected off the aluminum flyer. A VISAR velocity profile from a liquid CO_2 experiment is shown on the right in Fig. 3.3. The VISAR is able to track the aluminum flyer velocity up to impact on the sapphire drive plate. After impact, a shock is produced in the sapphire drive plate, but the shock is not strong enough to generate a reflective shock front. However, as the shock transits into the quartz, the quartz window melts into a conducting fluid and the velocity of the shock front is measured directly by the VISAR [15] as indicated in the Figure 3.3. As the shock transits into the liquid CO_2, the CO_2 dissociates and an insulator to metallic transition occurs causing the shock front in the CO_2 to be reflective. The reshock into the rear quartz window also creates a reflective shock front in the quartz, but the reshock data is not discussed in this report.

For the majority of the experiments, the measured quantities are the shock velocity in the quartz drive plate and the shock velocity in the CO_2 sample. The Hugoniot state of the quartz drive plate is determined from the measured shock velocity and a weighted cubic fit to the Z quartz Hugoniot data[15]. The CO_2 Hugoniot state is then determined using *Monte Carlo* Impedance matching methods and the reflected quartz Hugoniot. However, using the reflected quartz Hugoniot produces results that are soft compared to the true response of CO_2. Thus it is necessary to understand the release path of quartz. The quartz release path has been determined using DFT methods for several points along the Hugoniot and is validated by deep release data [16]. Figure 3.4 shows the quartz release effect compared to the reflected Hugoniot. The low impedance of CO_2 means the reflected versus release effect is greater and needs to be included in the impedance match calculations for accurate results. In two experiments, the front two-piece top hat was replaced with a single sapphire window. Fewer data exist for the Hugoniot of sapphire in the region of interest,

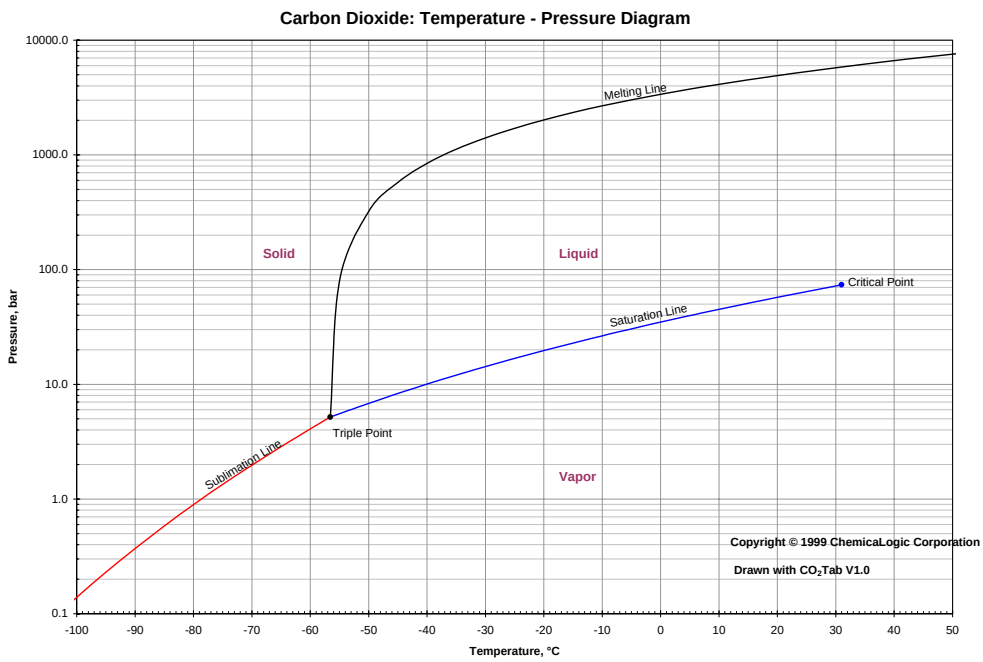

Figure 3.2. Phase diagram of CO_2

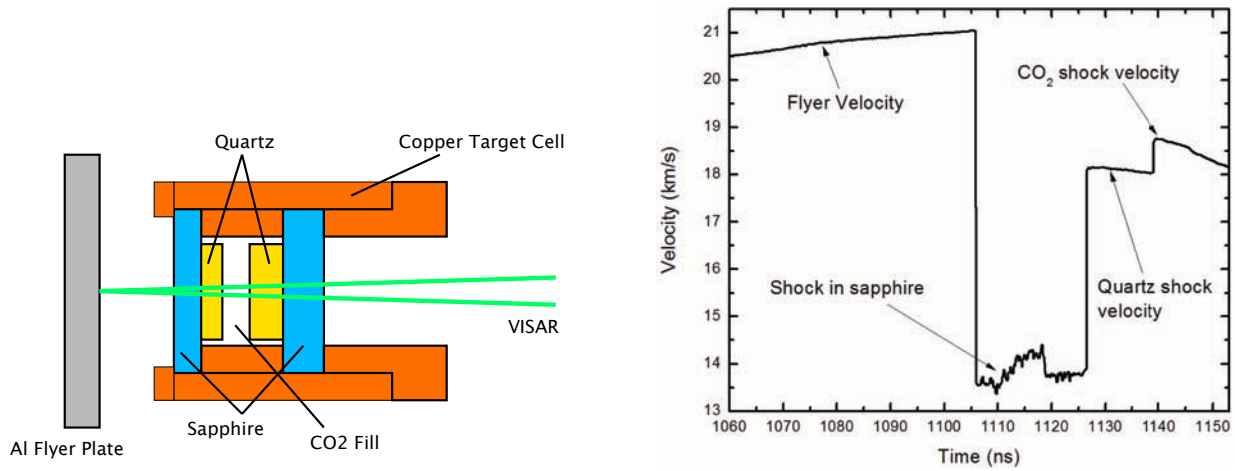

Figure 3.3. Schematic view of the flyer-plate impact experiment showing the front and rear two piece sapphire-quartz top-hat assembly. The flyer approach to the target is measured to high precision using VISAR. As seen on the right, the flyer is tracked up to impact. At impact the shock transits into the sapphire window, which does not have a reflective shock front. When the shock transits into the quartz window, the VISAR begins tracking the shock front (measuring the shock velocity directly) as it progresses through the quartz window. The shock transition into the CO_2 is also reflective and the shock velocity is measured directly. The direct measurements of the shock velocity in the quartz and CO_2 lead to high - precision, highly accurate determinations of the Hugoniot state.

Table 3.1. Cubic fit parameters for the Z-quartz Hugoniot data: $U_S = C_3U_P^3 + C_2U_P^2 + C_1U_P + C_0$

C_3	C_2	C_1	C_0
$6.979x10^{-4} \pm 3.244x10^{-4}$	-0.03844 ± 0.01031	1.9147 ± 0.1008	1.5591 ± 0.2976

Table 3.2. Linear fit parameters to the C-cut sapphire Hugoniot data: $U_S = C_0 + S_1U_P$

C_0	S_1
9.642 ± 0.175	1.089 ± 0.013

which leads to larger uncertainty. Table 3.2 lists the fit parameters from a weighted fit of known sapphire data [17]. The release of sapphire was determined using the tabular EOS SESAME 7420.

The quartz release correction was applied in the following manner:

1. The CO_2 Hugoniot state is calculated using the *Monte Carlo* impedance matching method and the reflected quartz Hugoniot. The quartz Hugoniot is a weighted, cubic fit to the Z experimental data and includes the fit parameter uncertainty and correlation.

2. In $P - U_P$ space, we plot both the quartz reflected Hugoniot and the calculated quartz release path from several known Hugoniot states. Also plotted is the the curve $P = \rho_0 U_S U_P$ where ρ_0 is the initial density of liquid argon and U_S is the measured value of the shock velocity in argon.

3. From the plot, we calculate the intercepts of the CO_2 curve $P = \rho_0 U_S U_P$ and the reflected and release quartz paths.

4. ΔU_P between the reflected Hugoniot and the release path is determined and a linear fit of the ΔU_P vs. $U_P(reflected)$ is performed.

5. Using the U_P calculated using the reflected Hugoniot and the linear fit calculated above, we can determine the correction to U_P needed to account for the quartz release path. This U_P and the measured U_S are used to calculate the final Hugoniot state pressure and density. The uncertainty in the data does not include the uncertainty in the release path as of this report.

Two Hugoniot data points were determined from impedance matching to sapphire. The impedance matching procedure was the same as described above. In this case, the initial shock velocity in the sapphire was determined from a transit time analysis. The sapphire release path was determined

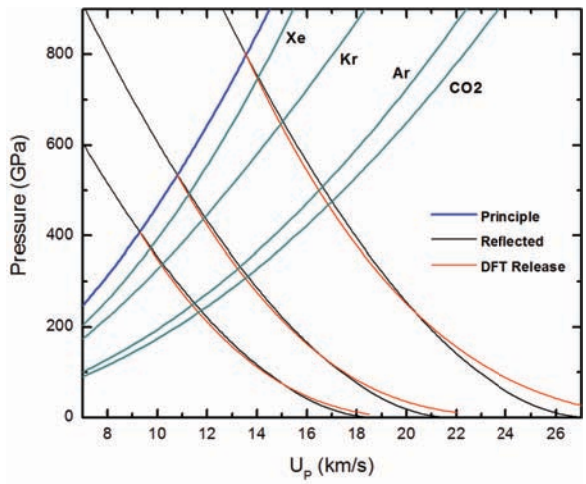

Figure 3.4. Comparison of the reflected Hugoniot and the DFT calculated release path for quartz at 3 initial pressure states. $P \quad U_P$ curves shown for 3 noble gases and CO_2 demonstrating the effect of using the reflected Hugoniot versus the release.

Table 3.3. Experimental data of the principal Hugoniot for shock compressed liquid CO_2 with an initial density of $1.167 g/cm^3$. The * indicates the data determined from impedance matching to a sapphire window.

Shot	$U_P(km/s)$	$U_S(km/s)$	$\rho(g/cm^3)$	$Pressure(GPa)$
Z2194-North	11.90 ± 0.05	17.34 ± 0.04	3.722 ± 0.042	240.9 ± 1.4
Z2194-South	12.99 ± 0.04	18.78 ± 0.03	3.785 ± 0.030	284.7 ± 0.9
Z2195-North	14.22 ± 0.05	20.48 ± 0.05	3.819 ± 0.042	339.9 ± 1.2
Z2195-South	15.25 ± 0.04	21.79 ± 0.06	3.890 ± 0.038	387.9 ± 1.3
Z2201-North*	15.82 ± 0.24	22.43 ± 0.05	3.961 ± 0.145	414.2 ± 6.3
Z2201-South*	16.78 ± 0.26	23.48 ± 0.06	4.090 ± 0.163	459.8 ± 7.3
Z2347-North	17.23 ± 0.06	24.23 ± 0.04	4.039 ± 0.042	487.2 ± 2.5
Z2347-South	18.19 ± 0.06	25.52 ± 0.04	4.066 ± 0.041	541.9 ± 2.7

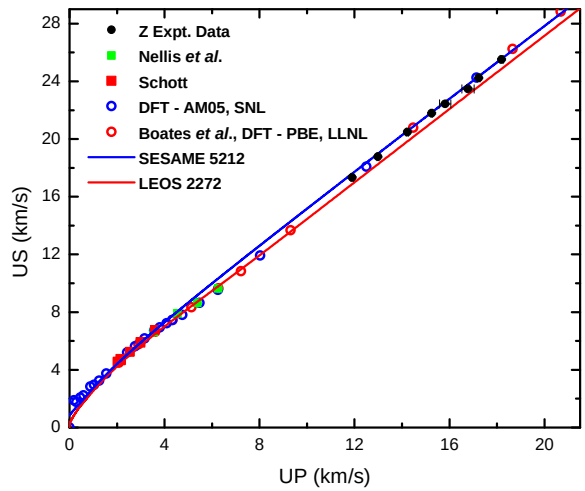

Figure 3.5. The $U_S - U_P$ data from the previously published data [18, 19], the DFT results from this work and Boates *et al.*[20], and the data collected from the Z experiments. The existing tabular EOS Hugoniot plots are also shown. For the experimental data, the uncertainty is on the order of the size of the data point.

using the SESAME 7420 table. Table 3.3 lists the experimental results for the principal Hugoniot of liquid CO_2.

Figures 3.5 and 3.6 show the Z experimental data in the $U_S - U_P$ and $\rho - P$ planes compared with the previous experimental data and the DFT simulation results discussed earlier. In the $U_S - U_P$ plane, the Z experimental data shows lower shock velocities than predicted by the SESAME 5212 model at lower velocities, but the table's agreement improves as the shock velocity increases. The LEOS 2272 table shows better agreement with the DFT results at particle velocities less than 10 km/s, but is too low above 10 km/s.

The differences between DFT simulations, tabular EOS models, and the experimental data are better observed in the more sensitive $\rho - P$ plane in Figure 3.6. For low pressures up to approximately 150 GPa, the LEOS table is in agreement with both sets of DFT simulations. Above 150 GPa, the LEOS table is too soft compared to the actual data. For pressures greater than 200 GPa both the SESAME 5212 and the DFT simulations are in good agreement with the Z experimental data. The effect of impedance matching to sapphire is clearly observed in the plot as well with that data having significantly larger error bars because of the uncertainty in the sapphire Hugoniot standard. The experimental data consistent to 550 GPa whether quartz or sapphire is used for impedance matching. Overall, the DFT simulations and the experimental data show that a new EOS model is needed for CO_2.

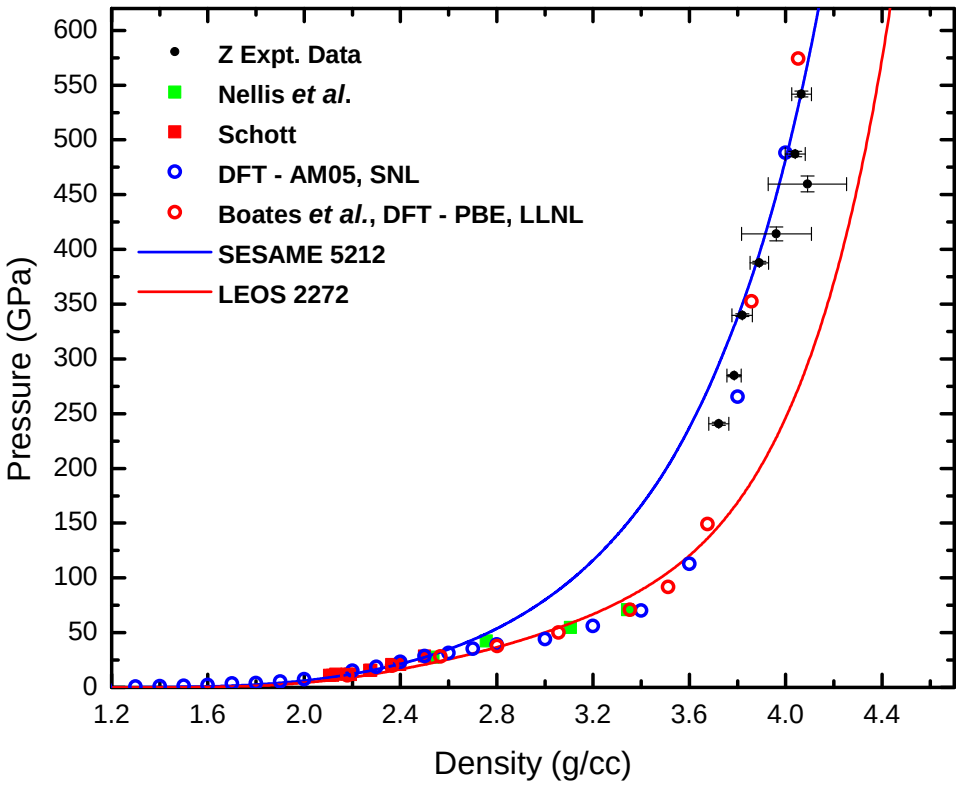

Figure 3.6. The $\rho - P$ Hugoniot data from all experimental data and the DFT simulation results. The existing tabular EOS Hugoniots are plotted as well showing the stiffer response of the models as compared to the data.

Chapter 4

Analysis of CO_2 tabular EOS models

With the new Hugoniot calculations and experimental data in hand, we now examine the behavior of four available EOS tables. Two tables are available from the LANL SESAME database as numbers 5211 and 5212, and two tables from LLNL, LEOS 2272 and 2274. Table 5211 was developed nearly 20 years ago with the aim of describing the fluid state at low temperatures. It does not include effects of dissociation and ionization and is tabulated over a limited range, up to 20,000 K. The 5212 table was developed more recently to extend the results of 5211 to higher temperatures and uses essentially the same model as in 5211. However, the tabulation is different, resulting in slightly different behavior as will be seen later. The LEOS tables were also developed recently and include a new model for molecular dissociation aimed at improving the behavior of the high pressure Hugoniot. Furthermore, LEOS 2274 utilized the DFT and experimental data presented earlier in the construction of the Hugoniot. In the following we will examine the agreement of these models with various sets of experimental and calculation data.

4.1 Shock Compression

The shock compression results for the EOS models from an initial liquid state are shown in Fig. 4.1. The onset of dissociation is evident around 40 GPa, where the Hugoniot softens in relation to its trend at lower pressures. The 5211 and 5212 models capture the behavior below dissociation quite well. However, as their descriptions note, they do not include dissociation and thus do not describe the softening behavior. Both 2272 and 2274 slightly underestimate the Hugoniot pressure below 40 GPa. They include dissociation models, and do agree better with the data than 5211 or 5212 in the dissociation regime, although there is still significant discrepancies with both the experimental data and DFT-MD calculations. Furthermore, despite having a dissociation model, these tables do not include an abrupt softening feature like the experimental data.

At higher pressures, the 5211 table cannot be used as it does not tabulate data above 20 kK. However, the extended version 5212 does intersect again with the Hugoniot data around 500 GPa, although with an incorrect slope. Here 2272 is much too soft, while 2274 is in very good agreement with both the experimental and calculation data.

Although the temperature along the Hugoniot has not been measured experimentally, the models may be compared with the temperature results from calculations, as shown in Fig. 4.2. Despite

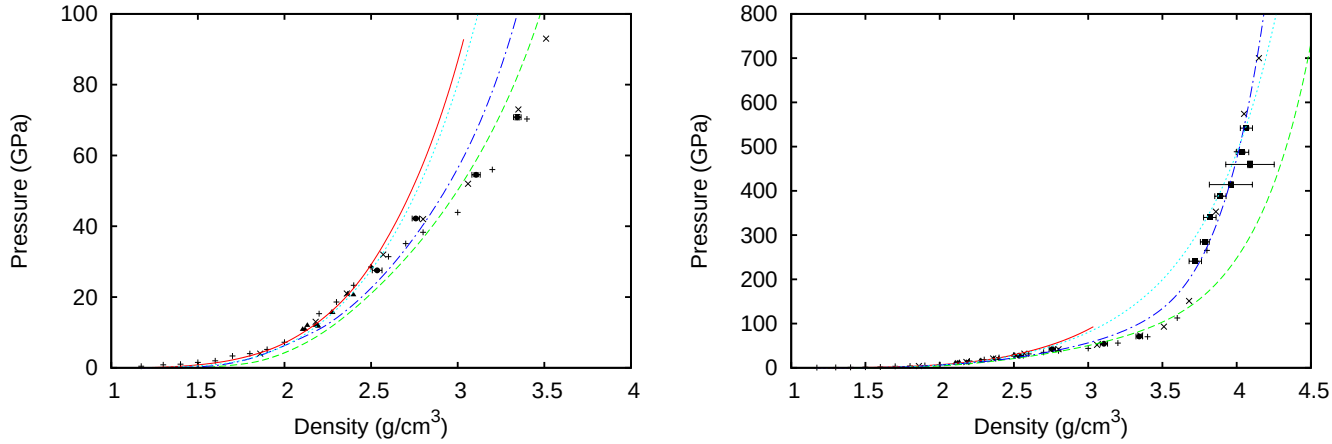

Figure 4.1. Shock compression results for CO_2 with initial liquid state at 1.73 g/cm^3 and 218 K. The left plot shows the low pressure and the right the high pressure region. Experimental data is shown as circles [18], diamonds [19], and the Z data of Ch. 3 as squares. DFT calculations from Ch. 2 are shown as exes, and pluses are from Ref. [20]. The models are shown as a solid red line (5211), a dotted cyan line (5212), a dashed green line (2272), and a dot-dash blue line (2274).

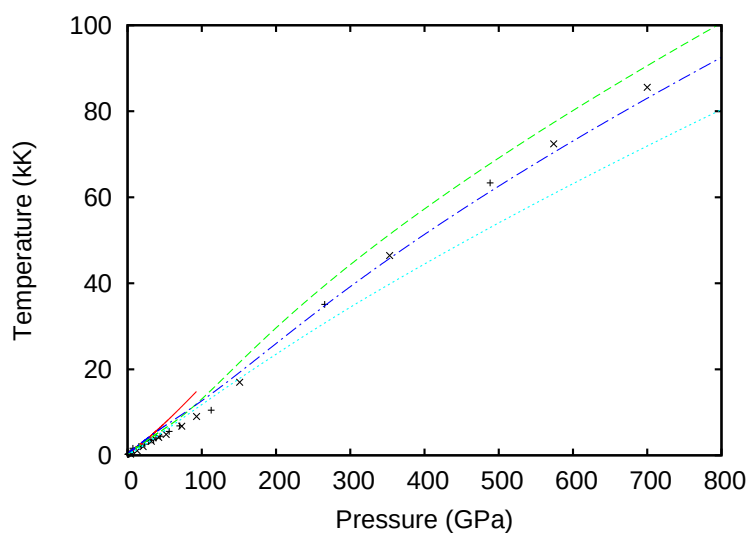

Figure 4.2. Shock temperature results for CO_2. Data and lines are as in Fig. 4.1.

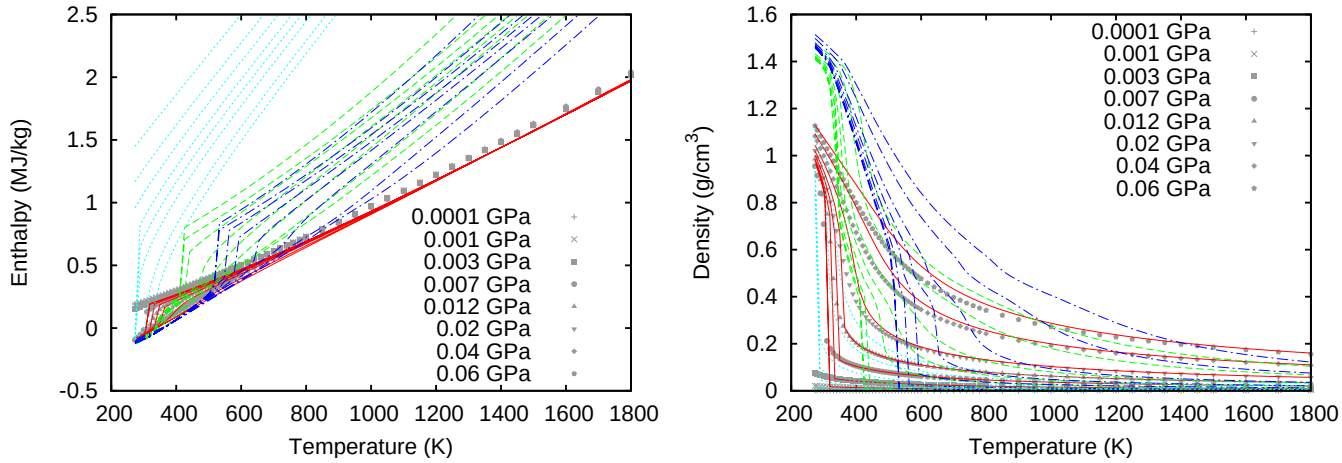

Figure 4.3. Isobaric expansion of fluid CO_2. Enthalpy is shown on the left with density in the right plot. Data is taken from Ref. [21]. Lines are as in Fig. 4.1. Model enthalpies are shifted so that all correspond at 0.06 GPa and 273.15 K.

its agreement with the pressure-density data, the 5211 model has a Hugoniot temperature that is much higher than the calculations. The 5212 model does better, but still overestimates the temperature near dissociation, and then underestimates it at high pressures, even in the region where it agrees with the pressure-density data. The 2272 model consistently overestimates the temperature by several thousand degrees. As with the pressure-density data, the 2274 model does best at high pressures, lying close to the calculations, although at low pressures it overestimates the temperature in the dissociation regime.

4.2 Fluid Isobars

The thermophysical properties of non-dissociated fluid CO_2 have been extensively measured. A subset of that data for the enthalpy and density is shown in Fig. 4.3 for a variety of pressures. Here model 5211 is a clear winner. Qualitatively, it agrees with the trends of both the enthalpy and density data, slightly overestimating the latter at low temperatures along the pressure isobars. The enthalpy behavior of all the other models can be seen to not even agree qualitatively with the data. Similarly, with the density, the other tables have large errors across the entire range of measured temperatures and pressures. The discrepancies between 5211 and 5212 are somewhat surprising as the descriptions of the table indicate that they should be using the same model. It would be surprising, although not out of the realm of possibility, that these differences were solely due to the choice of tabulation grid.

	T_c (K)	ρ_c (g/cm^3)	P_c (MPa)
Expt.	304.2	0.468	7.38
5211	361.3	0.477	13.25
5212	309.2	0.721	39.72
2272	458.7	0.230	5.30
2274	649.4	0.269	12.43

Table 4.1. Critical points for CO_2. The experimental values are given along with the four EOS tables under comparison. Experimental values are from Ref. [21] and have estimated error of less than one percent. Table results are as measured from interpolated pressure isotherms.

4.3 Phase boundaries

The melt curve of CO_2 has been mapped out accurately to 12 GPa using a laser heated DAC [13]. For the tables in question, the enthalpy at constant pressure was visually examined below 12 GPa over the temperature range 200-900 K, without significant evidence of the expected enthalpy change upon melting. The 2272 table did have a small signature of this jump, but it would be difficult to classify it as a melt transition. Thus, the tables appear to not include a melt region, at least anywhere near the experimentally measured curve.

All four tables do include van der Waals loops, which describes the vaporization of CO_2. The critical points for the termination of the vapor pressure curve were measured for each table by visually examining interpolated isotherms. The results are shown in Tab. 4.1. Clearly none of the tables describe the critical point well, although, 5211 is relatively close to the three critical parameters. The entire vapor curve has also been mapped experimentally. These results are shown in Fig. 4.4. The 5211 table gets close to the correct vapor curve, except at the higher temperatures, where it has too large of a critical point temperature and pressure. At low temperatures, 5212 almost meets the vapor pressure data, but is significantly off at higher temperatures, despite having a critical temperature that is withing two percent of the experimental value. The coexistence density is qualitatively described by both 5211 and 5212. The 5212 model is closer to the data, due to having a lower critical point temperature in the model, but has a curious non-symmetric behavior. Both the 2272 and 2274 models are grossly in error with the vaporization data.

4.4 Recommendations

There is no clear best EOS table for CO_2 among the ones examined in this Chapter. The choice of a table for simulations must be made carefully, with analysis of what areas are important for

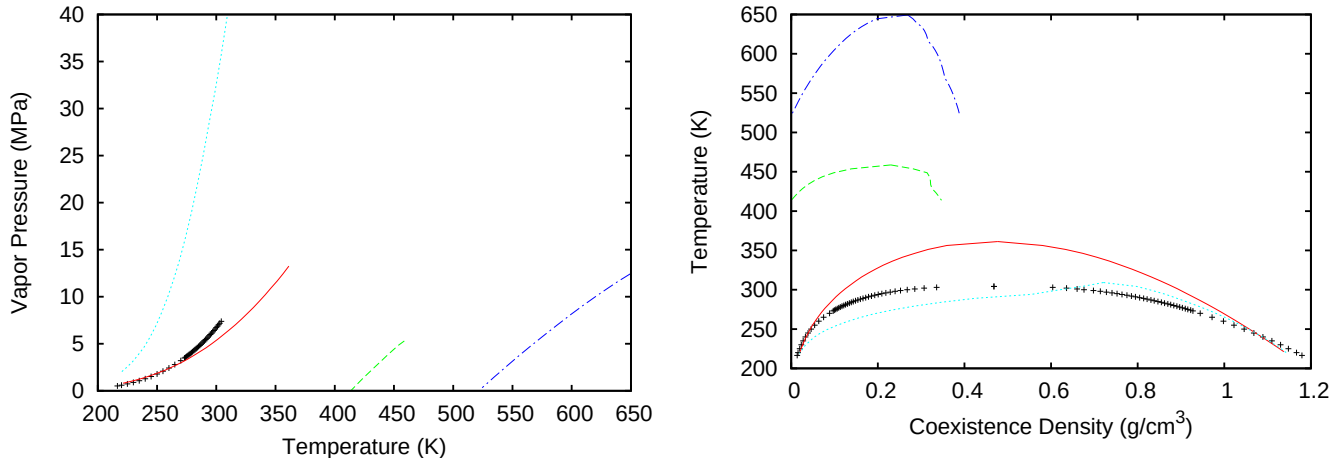

Figure 4.4. Vaporization results for CO_2. Experimental measurements taken from Ref. [21] are shown as pluses. Lines are as in Fig. 4.1. Model results are obtained from Maxwell constructions calculated from interpolated isotherms.

a particular application. At low pressures and temperatures, below 40 GPa and 4000 K, the 5211 model appears to be the best at giving a reasonable description of the non-dissociated fluid. Thus, it would seem to be the best choice among the four models in this regime.

At high pressures, above 200 GPa, only 2274 provides a good description of the shock response, and is the best choice. However, given its poor description of the low pressure, low temperature data, one should carefully examine that simulations are not significantly affected by errors accrued while material states traverse the non-dissociated regime.

In the dissociation regime between 40 and 200 GPa, none of the tables provide a good description of the data. Although 2272 lies nearest the shock data, due to its poor description of the data at both lower and higher pressures it is not really an acceptable table for use in this regime. Instead, 2274 should be used as the best available table, given its good agreement with the higher pressure data. Again, the same caveats as described in the preceding paragraph apply.

Chapter 5

Summary

We have completed an investigation into the response of CO_2 under shock compression. Initial work using DFT methods to predict the Hugoniot showed good agreement with the existing data to 50 GPa. The experiments performed using the Sandia Z machine extended the Hugoniot data to approximately 550 GPa. The experimental data validated the DFT simulations at multi-Mbar pressures. Furthermore, the DFT and Experimental results show that the existing EOS tables (SESAME 5211, SESAME 5212, LEOS 2272, and LEOS 2274) are likely inadequate for simulations extending over a wide-range of pressures. We recommend SESAME 5211 for simulations where dissociation is not present and LEOS 2274 for simulations where dissociation becomes important at high pressures. In the latter case, we include the caveat that one must check that errors accrued at low pressures do not adversely affect the simulation.

References

[1] S. Root, R. J. Magyar, J. H. Carpenter, D. L. Hanson, and T. R. Mattsson, Phys. Rev. Lett. **105**, 085501 (2010).

[2] M. Desjarlais, Phys. Rev. B **68**, 064204 (2003).

[3] M. D. Knudson *et al.*, Phys. Rev. Lett. **87**, 225501 (2001).

[4] M. D. Knudson, M. P. Desjarlais, and D. H. Dolan, Science **322**, 1822 (2008).

[5] P. Hohenberg and W. Kohn, Phys. Rev. **136**, B864 (1964).

[6] W. Kohn and L. J. Sham, Phys. Rev. **140**, A1133 (1965).

[7] N. Mermin, Phys. Rev. **137**, A1441 (1965).

[8] M. Allen and D. Tildesley, *Computer Simulations of Liquids* (Oxford Science Publications, 1987).

[9] M. E. Savage *et al.*, in *2007 IEEE Pulsed Power Conference* (2007), vol. 1-4, p. 979.

[10] S. Root *et al.*, krypton Hugoniot.

[11] D. L. Hanson, mini - cryostat design.

[12] R. Span and W. Wagner, J. Phys. Chem. Ref. Data **25**, 1509 (1996).

[13] V. M. Giordano, F. Datchi, and A. Dewaele, J. Chem. Phys. **125**, 054504 (2006).

[14] L. M. Barker and R. E. Hollenbach, J. Appl. Phys. **43**, 4669 (1972).

[15] M. D. Knudson and M. P. Desjarlais, Phys. Rev. Lett **103**, 225501 (2009).

[16] M. D. Knudson and M. P. Desjarlais, quartz release data and model.

[17] M. D. Knudson and S. Root, sapphire Hugoniot data and Monte Carlo Analysis.

[18] W. J. Nellis, A. C. Mitchell, F. H. Ree, M. Ross, N. C. Holmes, R. J. Trainor, and D. J. Erskine, J. Chem. Phys. **95**, 5268 (1991).

[19] G. L. Schott, High Press. Res. **6**, 187 (1991).

[20] B. Boates, S. Hamel, E. Schwegler, and S. A. Bonev, J. Chem. Phys. **134**, 064504 (2011).

[21] N. B. Vargaftik, *Tables on the Thermophysical Properties of Liquids and Gases in Normal and Dissociated States* (Hemisphere Publishing Corporation, Washington, D.C., 1975), p. 167.

DISTRIBUTION:

4 Lawrence Livermore National Laboratory
Phil Sterne
Cristine Wu
Lorin Benedict
Eric Schwegler

2 Los Alamos National Laboratory
Scott Crockett
Carl Greeff

1	MS 1323	Erik Strack, 1443
1	MS 1323	John Carpenter, 1443
1	MS 1190	Keith Matzen, 1600
1	MS 1189	Mark Hermann, 1640
1	MS 1189	Thomas Mattsson, 1641
1	MS 1189	Kyle Cochrane, 1641
1	MS 1189	Dawn Flicker, 1646
1	MS 1195	Seth Root, 1646
1	MS 0899	Technical Library, 9536 (electronic copy)

Sandia National Laboratories